JACS
JOURNAL OF THE AMERICAN CHEMICAL SOCIETY
Article
pubs.acs.org/JACS

A Planar Three-Coordinate Vanadium(II) Complex and the Study of Terminal Vanadium Nitrides from N_2: A Kinetic or Thermodynamic Impediment to N−N Bond Cleavage?

Ba L. Tran,[†] Balazs Pinter,[†] Adam J. Nichols,[†] Felicia T. Konopka,[†] Rick Thompson,[†] Chun-Hsing Chen,[†] J. Krzystek,[‡] Andrew Ozarowski,[‡] Joshua Telser,[§] Mu-Hyun Baik,[†] Karsten Meyer,[∥] and Daniel J. Mindiola*,[†]

[†]Department of Chemistry and Molecular Structure Center, Indiana University, Bloomington, Indiana 47405, United States
[‡]National High Magnetic Field Laboratory, Florida State University, Tallahassee, Florida 32310, United States
[§]Department of Biological, Chemical and Physical Sciences, Roosevelt University, Chicago, Illinois 60605, United States
[∥]Department of Chemistry and Pharmacy, Inorganic Chemistry, University of Erlangen-Nürnberg, Egerlandstrasse, 91058 Erlangen, Germany

Supporting Information

ABSTRACT: We report the first mononuclear three-coordinate vanadium(II) complex [(nacnac)V(ODiiP)] and its activation of N_2 to form an end-on bridging dinitrogen complex with a topologically linear V(III)N_2V(III) core and where each vanadium center antiferromagnetically couples to give a ground state singlet with an accessible triplet state as inferred by HFEPR spectroscopy. In addition to investigating the conversion of N_2 to the terminal nitride (as well as the microscopic reverse process), we discuss its similarities and contrasts to the isovalent d^3 system, [Mo(N[^{t}Bu]-Ar)$_3$], and the S = 1 system [(Ar[^{t}Bu]N)$_3$Mo]$_2$(μ_2-η^1:η^1-N_2).

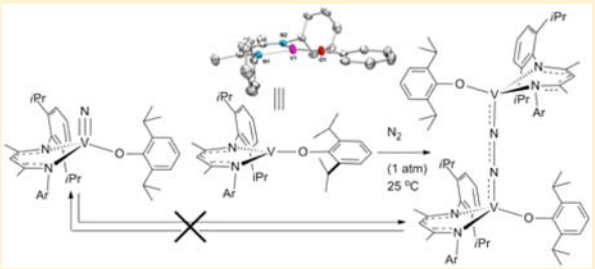

INTRODUCTION

Low-coordinate and electron-rich transition metal complexes have been long sought due to their potential utility in small molecule activation. One that illustrates the desired set of properties is the three-coordinate complex [Mo(N[^{t}Bu]Ar)$_3$] (Ar = 3,5-$Me_2C_6H_3$) reported by Cummins in 1995, which was shown to activate and cleave the triple bond of nitrogen, at 1 bar and 25 °C.[1−5] In a bimolecular fashion, this species can form two equivalents of nitride, [N≡Mo(N[^{t}Bu]Ar)$_3$]. Based on some diagonal relationship between Mo and V (their roles in nitrogenase enzymes, and some similar structural features in both low and high oxidation states), one may anticipate that the isovalent and three-coordinate V(II) complex will be comparably reactive. For example, three-coordinate V(III) complexes have been shown to reversibly sequester atmospheric nitrogen while V(II) systems can bind and break its triple bond, as well as convert nitrogen to ammonia.[6−9] Surprisingly, discrete examples of three-coordinate V(II) complexes have not been reported, with the closest reference being the masked system [(nacnac)V(Ntolyl$_2$)] (nacnac$^-$ = [ArNC(CH$_3$)]$_2$CH, tolyl = 4-MeC_6H_4, Ar = 2,6-^{i}Pr$_2$C$_6$H$_3$).[10] Complex [(nacnac)V(Ntolyl$_2$)] has a resting state displaying an arene interaction with the tolyl moiety (eq 1) and the system does behave as a three-coordinate V(II) fragment when treated with reagents such as PhCCPh, N_3Ad, S_8, P_4, pyridine N-oxide, PhXXPh (X = S or Se), and the N-atom source N≡Cr(O^{t}Bu)$_3$.[11,12] However, unlike unsaturated V(II) complexes generated by chemical and electrochemical reduction, [(nacnac)V(Ntolyl$_2$)] fails to bind N_2, presumably due to the blockade imposed by the tethered arene motif (eq 1). This suggests that the resting state of [(nacnac)V(Ntolyl$_2$)], even in the solution phase, is not in equilibrium with a three-coordinate fragment (eq 1), or that the V(II)−arene interaction is more favorable than V(II)−N_2 binding. The lack of *bona fide* examples of discrete three-coordinate V(II) complexes is surprising since such species would likely engage in N_2 activation and cleavage reactions.

In this work, we present the first example of a three-coordinate vanadium(II) complex. Its existence has been unequivocally established by a combination of characterization techniques including solid state magnetic studies (SQUID), high-frequency and -field EPR (HFEPR), and a single crystal structural analysis (XRD). In addition, we demonstrate this complex to be a reactive template, capable of activating N_2 to form a dinuclear complex displaying a singlet ground state (with an accessible triplet state) with an end-on dinitrogen ligand that bridges the two metal centers. Surprisingly, the divanadium dinitrogen complex does not fragment into two vanadium(V) nitride molecules despite the presence of a

Received: April 13, 2012
Published: June 13, 2012

dx.doi.org/10.1021/ja303360v | J. Am. Chem. Soc. 2012, 134, 13035−13045

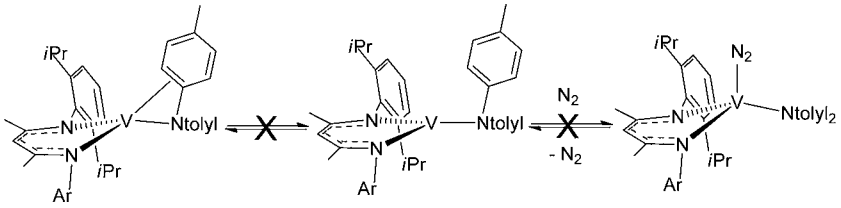

(1)

sufficient number of electrons to populate all the π^* and σ^* orbitals of N_2. The chemistry of this species contrasts that of isovalent $[Mo(N[^tBu]Ar)_3]$. Lastly, we present theoretical studies that point to the conversion of N_2 to two N^3-(nitride) to being both kinetically and thermodynamically prohibited.

EXPERIMENTAL DETAILS

General Considerations. Unless otherwise stated, all operations were performed in an M. Braun Lab Master double-drybox under an atmosphere of argon or nitrogen, or using high vacuum standard Schlenk techniques under a nitrogen or argon atmosphere. Anhydrous hexanes, *n*-pentane, toluene, and benzene were purchased from Aldrich in sure-sealed reservoirs (18 L) and dried by passage through two columns of activated alumina and a Q-5 column. Diethyl ether and CH_2Cl_2 were dried by passage through a column of activated alumina. THF was distilled, under nitrogen, from purple sodium benzophenone ketyl and stored under sodium metal. Distilled THF was transferred under vacuum into bombs before being pumped into a drybox. C_6D_6 was purchased from Cambridge Isotope Laboratory (CIL), degassed and vacuum transferred to 4 Å molecular sieves. Celite, alumina, and 4 Å molecular sieves were activated under vacuum overnight at 200 °C. All other chemicals were used as received from Sigma-Aldrich unless otherwise stated and 98% atom enriched $^{15}N_2$ was purchased from Cambridge Isotope Laboratories. ^1H, ^{13}C, ^{51}V, and ^{15}N NMR spectra were recorded on Varian 400 and 500 MHz NMR spectrometers. ^1H and ^{13}C NMR are reported with reference to solvent resonances of C_6D_6 at 7.16 and 128.0 ppm, respectively. ^{51}V NMR spectral values are reported with reference to neat $VOCl_3$. ^{15}N NMR spectral values are reported with reference to neat $MeNO_2$ (380.2 ppm). X-ray diffraction data were collected on a SMART6000 (Bruker) system under a stream of N_2(g) at 150 K. Elemental analysis was performed at Indiana University, Bloomington (CE Elantech Flash EA1112 Elemental Analysis System). All UV−vis spectroscopy experiments were recorded using a Perkin-Elmer Lambda 650 UV−vis Spectrometer under PC control equipped with Perkin-Elmer software and Peltier heating system. Infrared spectroscopy was performed on the Thermo Nicolet 6700 FT-IR equipped with software under PC control. Complex $[(nacnac)VCl_2]$ [nacnac$^-$ = $[ArNC(Me)]_2CH$, Ar = 2,6-^{i}Pr$_2$C$_6$H$_3$] was prepared according to published literature.[13] NaODiiP was obtained from HODiiP and $NaN(SiMe_3)_2$ in pentane or diethylether followed by filtration of the solid, washing with ether, and then drying under reduced pressure. Magnetic moments in solution were obtained by the method of Evans.[14] Warning: Na/Hg should be handled cautiously due to its potentially pyrophoric nature. NaN_3 should be handled cautiously due to its explosive nature. It is recommended that NaN_3 be purified by stirring the solids in dry THF overnight, filtering and washing the solid with copious amounts of THF, and then drying the white solid overnight under reduced pressure.

*Synthesis of (nacnac)VCl(ODiiP) (**1**).* In a 100 mL round-bottom flask, to a chilled toluene (50 mL) solution of $(nacnac)VCl_2$ (2.20 g, 4.08 mmol) was added solid NaODiiP (857 mg, 4.28 mmol) via spatula over 15 min. The yellow-green solution turned dark forest green. After stirring for 2 h, the reaction mixture was filtered through a medium porosity frit containing Celite to remove salt residues. Subsequently, all volatiles were removed under reduced pressure and addition of 50 mL of hexanes led to the precipitation of pure green solids which were collected on a medium porosity frit and dried under reduced vacuum. Reducing the volume of the filtrate to 20 mL and storage at −37 °C afforded additional dark green crystalline product, which was collected, and dried under reduced pressure. Yield = 76% (2.11 g, 3.09 mmol). ^1H NMR (25 °C, 400 MHz, C_6D_6): δ 10.26 ($\Delta\nu_{1/2}$ = 1069 Hz), 9.31 ($\Delta\nu_{1/2}$ = 176 Hz), 8.58 ($\Delta\nu_{1/2}$ = 1004 Hz), 6.95 ($\Delta\nu_{1/2}$ = 18 Hz), 4.04 ($\Delta\nu_{1/2}$ = 1360 Hz), 3.82 ($\Delta\nu_{1/2}$ = 1448 Hz), 3.25 ($\Delta\nu_{1/2}$ = 25 Hz), 2.97 ($\Delta\nu_{1/2}$ = 901 Hz), 1.66 ($\Delta\nu_{1/2}$ = 74 Hz), 1.22 ($\Delta\nu_{1/2}$ = 31 Hz), 1.10 ($\Delta\nu_{1/2}$ = 20 Hz), 0.86 ($\Delta\nu_{1/2}$ = 24 Hz), −5.80 ($\Delta\nu_{1/2}$ = 221 Hz). μ_{eff} = 2.78 μ_B (Evans, 25 °C). Anal. Calcd for $C_{41}H_{58}ClN_2OV$: C, 72.28; H, 8.58; N, 4.11. Found: C, 72.55; H, 8.50; N, 3.99.

*Synthesis of (nacnac)V(ODiiP) (**2**).* Under an argon atmosphere, a 250 mL flask was charged with **1** (640 mg, 0.94 mmol), toluene (50 mL), and 0.5% Na/Hg (27 mg, 1.17 mmol Na and 5.40 g Hg) at room temperature. After stirring for 8 h, the reaction mixture turned from dark green to brown. The supernatant was transferred via glass pipet (leaving behind the amalgam) to a 250 mL round-bottom flask and all volatiles removed. The crude product was extracted into *n*-pentane (75 mL), filtered through a medium porosity frit containing Celite to remove salt residues and washed with an additional 25 mL of *n*-pentane. Subsequently, the filtrate was reduced to 5 mL under vacuum, and storage of the concentrated solution at −35 °C afforded a dark-brown crystalline product, which was collected and dried under reduced pressure. Yield = 38% (245.4 mg, 0.38 mmol). ^1H NMR (25 °C, 400 MHz, C_6D_6): δ 20.81 ($\Delta\nu_{1/2}$ = 76 Hz), 11.61 ($\Delta\nu_{1/2}$ = 246 Hz), 8.95 ($\Delta\nu_{1/2}$ = 316 Hz), 3.47 ($\Delta\nu_{1/2}$ = 338 Hz), −4.78 ($\Delta\nu_{1/2}$ = 8759 Hz), −14.37 ($\Delta\nu_{1/2}$ = 279 Hz). μ_{eff} = 3.77 μ_B (SQUID, 25−300 K); 3.83 μ_B (Evans, 25 °C). Anal. Calcd for $C_{41}H_{58}N_2OV$: C, 76.25; H, 9.05; N, 4.34. Found: C, 76.55; H, 9.10; N, 4.11.

*Synthesis of (nacnac)V(DMAP)(ODiiP) (**3**).* In a 100 mL round-bottom flask was charged **1** (260.0 mg, 0.38 mmol), DMAP (49.0 mg, 0.40 mmol), and toluene (15 mL) and cooled to −37 °C. To the chilled round-bottom flask was added 0.5% Na/Hg (10.5 mg, 0.45 mmol Na and 2.09 g Hg). After stirring for 12 h, the reaction mixture turned from dark green to a darker color. The supernatant was transferred via glass pipet (leaving behind the amalgam) to a 100 mL round-bottom flask and all volatiles removed under reduced pressure. The crude product was extracted into diethyl ether (20 mL), filtered through a medium porosity frit containing Celite to remove salt residues. Subsequently, the ethereal solution (the filtrate) was reduced to 4 mL under vacuum and storage at −37 °C afforded a dark crystalline product, which was collected, and dried under reduced pressure. Yield = 65% (189.7 mg, 0.25 mmol). ^1H NMR (25 °C, 300 MHz, C_6D_6): δ 32.93 ($\Delta\nu_{1/2}$ = 176 Hz), 26.00 ($\Delta\nu_{1/2}$ = 200 Hz), 14.34 ($\Delta\nu_{1/2}$ = 70 Hz), 8.47 (overlap), 7.80 (overlap), 5.64 ($\Delta\nu_{1/2}$ = 1676 Hz), 4.06 ($\Delta\nu_{1/2}$ = 1240 Hz), 2.74 ($\Delta\nu_{1/2}$ = 719 Hz), 2.10 ($\Delta\nu_{1/2}$ = 10 Hz), 0.87 ($\Delta\nu_{1/2}$ = 12 Hz), −1.39 ($\Delta\nu_{1/2}$ = 146 Hz), −14.12 ($\Delta\nu_{1/2}$ = 47 Hz). μ_{eff} = 3.79 μ_B (Evans, 25 °C). Anal. Calcd for $C_{48}H_{68}N_4OV$: C, 75.06; H, 8.92; N, 7.29. Found: C, 75.25; H, 8.85; N, 7.52.

*Synthesis of [(nacnac)(ODiiP)V]$_2$(μ_2-η^1:η^1-N$_2$) (**4**).* In a 250 mL round-bottom flask was charged **1** (2.00 g, 2.94 mmol), toluene (50 mL), and 0.5% Na/Hg (84.3 mg, 3.67 mmol Na/16.8 g Hg) at room temperature. After stirring for 12 h, the reaction mixture turned from dark green to brown. The supernatant was transferred via glass pipet (leaving behind the amalgam) to a 250 mL round-bottom flask and all volatiles removed. The crude product was extracted into *n*-pentane (75 mL) filtered through a medium porosity frit containing Celite to remove salt residues and washed with additional 25 mL of *n*-pentane. (***Note***: the insoluble brown solid atop the porous frit is an undesired side product). Subsequently, the filtrate was reduced to 15 mL under vacuum, and storage of the concentrated solution at −35 °C afforded a dark-brown crystalline product, which was collected and dried under reduced pressure. Yield = 60% (1.16 g, 0.88 mmol). ^1H NMR (25 °C,

dx.doi.org/10.1021/ja303360v | J. Am. Chem. Soc. 2012, 134, 13035−13045

400 MHz, C_6D_6): δ 7.71 ($\Delta\nu_{1/2}$ = 27 Hz), 7.48 ($\Delta\nu_{1/2}$ = 29 Hz), 7.26 ($\Delta\nu_{1/2}$ = 20 Hz), 7.05 ($\Delta\nu_{1/2}$ = 26 Hz), 6.97 ($\Delta\nu_{1/2}$ = 55 Hz), 6.86 ($\Delta\nu_{1/2}$ = 24 Hz), 6.72 ($\Delta\nu_{1/2}$ = 20 Hz), 6.39 ($\Delta\nu_{1/2}$ = 20 Hz), 5.69 ($\Delta\nu_{1/2}$ = 28 Hz), 3.27 ($\Delta\nu_{1/2}$ = 122 Hz), 3.10 ($\Delta\nu_{1/2}$ = 132 Hz), 1.77 ($\Delta\nu_{1/2}$ = 537 Hz), 1.62 ($\Delta\nu_{1/2}$ = 429 Hz), 1.42 ($\Delta\nu_{1/2}$ = 29 Hz), 0.65 ($\Delta\nu_{1/2}$ = 555 Hz). ^{51}V NMR (25 °C, 131.5 MHz, C_6D_6): δ 167 ($\Delta\nu_{1/2}$ = 500 Hz). Raman (785 nm excitation): 1374 ($^{14}N_2$), 1330 ($^{15}N_2$) cm^{-1}. Anal. Calcd for $C_{82}H_{116}N_6O_2V_2$: C, 74.63; H, 8.86; N, 6.37. Found: C, 74.55; H, 8.75; N, 6.50.

Synthesis of 4-$^{15}N_2$. Under Ar atmosphere a 100 mL Schlenk flask was charged with **1** (500.0 mg, 0.73 mmol), toluene (25 mL), and 0.5% Na/Hg (21.0 mg, 0.92 mmol Na and 4.22 g Hg) at 25 °C. The Schlenk flask was removed from the glovebox and attached to a Schlenk line. The flask underwent two cycles of freeze, pump, and thaw. To the frozen solution was added $^{15}N_2$ (1 atm) and the reaction mixture was allowed to reach 25 °C. After stirring for 12 h, the reaction mixture turned from dark green to yellow-brown. The flask was taken back into the argon glovebox for workup. The supernatant was transferred via glass pipet (leaving behind the amalgam) to a 100 mL round-bottom flask and all volatiles were removed under reduced pressure. The crude product was extracted into *n*-pentane (20 mL), filtered through a medium porosity frit containing Celite to remove salt residues. Subsequently, the *n*-pentane solution was reduced in volume under vacuum and storage of the concentrated solution at −37 °C afforded a crystalline product, which was collected, and dried under reduced pressure. Yield = 63% (607 mg, 0.46 mmol). The dinitrogen product was confirmed by ^{1}H and ^{51}V NMR spectral matching that of **4** as well as by IR spectroscopic data.

*Synthesis of (nacnac)V≡N(ODiiP) (**5**).* In a 100 mL round-bottom flask was charged **1** (1.00 g, 1.47 mmol), 75 mL of THF, and solid NaN_3 (573.3 mg, 8.82 mmol). After stirring for 6 h, all volatiles from the reaction mixture were removed under reduced pressure and the crude material was extracted with 50 mL of toluene and filtered through a medium porosity frit containing Celite to remove excess NaN_3 and salt residues. Subsequently, the resulting filtrate was transferred into a thick walled glass reaction vessel equipped with a Telfon cap, a large stirring bar, and heated to 60 °C for 12 h in an oil bath. Removal of all volatiles and addition of hexanes (10 mL) led to the precipitation of yellow crystalline material that was collected on a medium porosity frit, rinsed with hexanes (5 mL) and dried under reduced vacuum to yield a clean product. Yield = 70% (679 mg, 1.02 mmol). ^{1}H NMR (25 °C, 400 MHz, d_8-toluene): δ 7.18−7.6.95 (m, 9H, Ar-*H*), 5.66 (br, ($\Delta\nu_{1/2}$ = 149 Hz, 1H, O{2,6-C*H*(CH_3)$_2$-C_6H_3), 4.98 (s, 1H, α-H), 4.04 (septet, 2H, C*H*(CH_3)$_2$), 2.90 (br, ($\Delta\nu_{1/2}$ = 200 Hz, 1H, O{2,6-C*H*(CH_3)$_2$-C_6H_3), 2.67 (septet, 2H, C*H*(CH_3)$_2$), 1.58 (s, 6H, ArN(C*H*$_3$)CCHC(C*H*$_3$)NAr), 1.47 (d, J_{H-H} = 6 Hz, 6H, CH(C*H*$_3$)$_2$), 1.25 (br, $\Delta\nu_{1/2}$ = 98 Hz, 12H, O{2,6-CH(C*H*$_3$)$_2$-C_6H_3)), 1.18 (d, J_{H-H} = 7 Hz, 6H, CH(C*H*$_3$)$_2$), 1.15 (d, J_{H-H} = 7 Hz, 6H, CH(C*H*$_3$)$_2$), 1.02 (d, J_{H-H} = 7 Hz, 6H, CH(C*H*$_3$)$_2$). ^{1}H NMR (−40 °C, 400 MHz, *d*-toluene): δ 7.28 (d, J_{H-H} = 7 Hz, 1H, Ar-*H*), 7.07−7.00 (m, 7H, Ar-*H*), 6.95 (d, J_{H-H} = 7 Hz, 1H, Ar-*H*), 5.75 (m, 1H, C*H*(CH_3)$_2$), 4.79 (s, 1H, α-H), 4.10 (m 2H, C*H*(CH_3)$_2$), 2.92 (m, 1H, C*H*(CH_3)$_2$), 2.63 (m, 2H, C*H*(CH_3)$_2$), 1.51 (d, J_{H-H} = 6 Hz, CH(C*H*$_3$)$_2$), 1.43 (s, 6H, ArN(C*H*$_3$)CCHC(C*H*$_3$)NAr), 1.39 (d, J_{H-H} = 6 Hz, CH(C*H*$_3$)$_2$), 1.18 (m, 18H, CH(C*H*$_3$)$_2$), 1.06 (d, J_{H-H} = 6 Hz, CH(C*H*$_3$)$_2$). ^{13}C{^{1}H} NMR (25 °C, 100 MHz, C_6D_6): δ 170.1 (ArN(CH_3)CCHC(CH_3)NAr), 146.1 (Ar), 142.4 (Ar), 142.3 (Ar), 125.1 (Ar), 124.5 (Ar), 121.7 (Ar), 98.8 (ArN(CH_3)CCHC(CH_3)-NAr), 29.3 (CH(CH_3)$_2$), 28.8 (CH(CH_3)$_2$), 26.3 (CH(CH_3)$_2$), 24.9 (CH(CH_3)$_2$), 24.7 (ArN(CH_3)CCHC(CH_3)NAr)), 24.2 (CH-(CH_3)$_2$), 24.0 (CH(CH_3)$_2$). ^{51}V NMR (25 °C, 131.5 MHz, C_6D_6): δ −219.7 ($\Delta\nu_{1/2}$ = 1308 Hz). FT−IR (KBr, Nujol, cm^{-1}): 1024 (V≡N), 998 (V≡N^{15}). ^{15}N (25 °C, 50.6 MHz, C_6D_6): δ 1058.7 ($\Delta\nu_{1/2}$ = 36.0 Hz). Anal. Calcd for $C_{41}H_{58}N_3OV$: C, 74.63; H, 8.86; N, 6.37. Found: C, 74.65; H, 8.75; N, 6.15. The synthesis of the ^{15}N isotopomer, [(nacnac)V≡^{15}N(ODiiP)] was prepared following the same procedure above by using 50% enriched $Na^{15}N_3$.

Thermolysis and Photolysis Experiments. For the thermolysis experiment, a J-Young NMR tube containing **4** in C_6D_6 was placed into a preheated oil bath at 90 °C. The reaction was monitored by ^{1}H NMR spectroscopy. Complex **2** was confirmed as the product by comparison to a ^{1}H NMR (25 °C, C_6D_6) spectrum of authentic **2**. For the photolysis experiment, a J-Young NMR tube containing **4** in C_6D_6 was placed into a circulating water bath (25 °C) equipped with a mercury lamp and monitored by ^{1}H NMR spectroscopy, which confirmed formation of **2**, as in the thermolysis experiment.

Cyclic Voltammetry Measurement of [(nacnac)VCl(Ntol$_2$)]. Cyclic voltammetry was performed in 0.3 M of predried and recrystallized *n*-tetrabutylammonium hexafluorophosphate ($TBAPF_6$) in anhydrous THF solution. Commercial $TBAPF_6$ was recrystallized from boiling ethanol and cooling to 25 °C gave large colorless needles. The crystals were collected on a frit and washed with cold ethanol, and pure crystals of $TBAPF_6$ were dried under reduced pressure at 25 °C for 48 h. A platinum disk (2.0 mm diameter), a platinum wire, and silver wire were employed as the working electrode, the auxiliary, and the reference electrode, respectively. A one compartment cell was used in the CV measurements. The electrochemical response was collected with the assistance of an E2 Epsilon (BAS) autolab potentiostat/galvanostat under control by BAS software. All of the potentials were reported against the Fc^+/Fc couple (0.0 V). The IR drop correction was applied when significant resistance was noted. The spectrum was recorded under an N_2 atmosphere in the glovebox. In a typical experiment, 20 mg of crystalline sample of **1** or **4** was dissolved in 5 mL of a $TBAPF_6$ solution in THF at 25 °C.

Magnetic Susceptibility Measurements. Magnetic data were collected on a Quantumn Design MPMS-XL SQUID magnetometer. All dc susceptibility measurements were obtained on three independently synthesized microcrystalline powders placed in gelatin capsules. Measurements were collected with a temperature range of 2−300 K under a dc field of 1 T. All samples were corrected for diamagnetic contributions using Pascal's constants.[15]

HFEPR Data Acquisition and Sample Preparation. High-frequency and -field electron paramagnetic resonance (HFEPR) spectra were recorded using the Electron Magnetic Resonance (EMR) Facility at the National High Magnetic Field Laboratory (NHMFL, Tallahassee, FL). The spectrometer employs a Virginia Diodes (Charlottesville, VA) source operating at a base frequency of 12−14 GHz and multiplied by a cascade of multipliers in conjunction with a 15/17 T superconducting magnet.[16] Detection was provided with an InSb hot-electron bolometer (QMC Ltd., Cardiff, U.K.). The magnetic field was modulated at 50 kHz. A Stanford Research Systems SR830 lock-in amplifier converted the modulated signal to DC voltage. Low temperature was provided by a continuous flow cryostat with a temperature controller (both Oxford Instruments (Oxford, U.K.)). Well-ground solid powder samples of complex **2** or **4** (typically, 30−50 mg) were loaded into sample holders under argon atmosphere. During this process, and in subsequent, albeit rapid, transfer to the sample holder followed by freezing in liquid nitrogen, it is likely that some air oxidation of V(II) to paramagnetic V(III) and V(IV) species (and perhaps even to diamagnetic V(V)) occurred.

Raman Spectroscopy Details. Raman data were recorded using a Renishaw inVia Raman microscope fitted with a diode laser (Renishaw) for 785 nm excitation. The instrument was interfaced with a light microscope fitted with a 50× objective (Leica; numerical aperture 0.5) focused into a cuvette containing the solution (Starna, Spectrosil grade quartz). The spectrometer was wavelength-calibrated using silicon (520.5 cm^{-1}). Laser powers used in the experiments were adjusted with neutral density filters to ensure sample integrity for the duration of each experiment, usually 30 mW. No corrections for spectrometer sensitivity were conducted. The sample was recorded based on the following parameters: 100−3300 cm^{-1}; 10 s/1000 cm^{-1}; 15 mW; λ_{ex} = 785 nm.

Computational Details. All calculations were carried out using DFT as implemented in the Jaguar 7.7 suite[17] of *ab initio* quantum chemistry programs. Geometry optimizations were performed with the B3LYP[18−21] functional and the 6-31G** basis set. Vanadium was represented using the Los Alamos LACVP basis[22,23] that includes effective core potentials. The energies of the optimized structures were reevaluated by additional single point calculations on each optimized geometry using Dunning's correlation consistent triple-ζ basis set[22] cc-

pVTZ(-f) that includes a double set of polarization functions. For V, we used a modified version of LACVP, designated as LACV3P, in which the exponents were decontracted to match the effective core potential with triple-ζ quality. Solvation energies were evaluated by a self-consistent reaction field[25−27] (SCRF) approach based on accurate numerical solutions of the Poisson−Boltzmann equation. In the results reported, solvation calculations were carried out with the 6-31G**/LACVP basis at the optimized gas-phase geometry employing the dielectric constant of ε = 2.284 for benzene. As is the case for all continuum models, the solvation energies are subject to empirical parametrization of the atomic radii that are used to generate the solute surface. We employed[28] the standard set of optimized radii in Jaguar for H (1.150 Å), C (1.900 Å), N (1.600 Å) and V (1.572 Å). Analytical vibrational frequencies within the harmonic approximation were computed with the 6-31G**/LACVP basis to confirm proper convergence to well-defined minima or saddle points on the potential energy surface.

Convergence to plausible electronic states that correspond to conceptually meaningful electronic configurations was monitored by carefully observing the Mulliken spin densities and visualizing the frontier molecular orbitals. When multiple minima were encountered, we compared the total energies and chose the structure with the lowest energy. Antiferromagnetically (AF) coupled states were modeled using Noodleman's broken symmetry (BS) formalism without spin projection,[29−31] as the spin projection corrections are uniformly found to be negligibly small. The energy components have been computed with the protocol below. The free energy in solution phase G(Sol) has been calculated as follows:

$$G(\mathrm{Sol}) = G(\mathrm{gas}) + G^{\mathrm{solv}} \quad (1)$$

$$H(\mathrm{gas}) = E(\mathrm{SCF}) + E_t + E_r + E_v + k_B T \quad (2)$$

G(gas) is the free energy in gas phase; G^{solv} is the free energy of solvation as computed using the continuum solvation model; H(gas) is the enthalpy in gas phase; T is the temperature (298.00K); E(SCF) is the self-consistent field energy, that is, "raw" electronic energy as computed from the SCF procedure and the contributions of translational, rotational and vibrational motions to the enthalpy respectively are E_t = 3/2RT, E_r = 3/2RT (RT, for linear molecules) and $E_v = R\Sigma_K\Theta_{v,K}(1/2 + 1/(e^{\Theta_{v,K}/T}-1))$, where $\Theta_{v,K} = h\nu_K/k_B$. Note that by entropy here we refer specifically to the vibrational/rotational/translational entropy of the solute(s); the entropy of the solvent is incorporated implicitly in the continuum solvation model. To locate transition states, the potential energy surface was first explored approximately using the linear synchronous transit (LST)[32] method, followed by a quadratic synchronous transit (QST)[33] search using the LST geometry as an initial guess.

RESULTS AND DISCUSSION

Complexes of vanadium(II)[34,35] and vanadium(III)[36−39] have been reported to bind and activate dinitrogen; however, only transient vanadium(II) species generated under reducing conditions have been implicated in the cleavage of dinitrogen.[35,40,41] Against this backdrop, we geared our efforts toward the isolation of a well-defined vanadium(II) species to investigate its electronic structure and interaction with dinitrogen. Recently, we reported the isolation of a masked three-coordinate V(II) fragment, [(nacnac)V(Ntol$_2$)], but such a complex failed to bind dinitrogen, likely due to the interaction of tolyl arene with the coordinately unsaturated metal center as noted in the solid state structural diagram (eq 1).[10] Consequently, we sought to disfavor the metal-arene interaction by replacing the ditolylanilide with 2,6-diisopropylphenoxide (ODiiP). The reaction of [(nacnac)VCl$_2$][13] and NaODiiP produced [(nacnac)VCl(ODiiP)] (**1**) in 70% isolated yield as a green solid (Scheme 1). Complex **1** can be prepared in multigram quantities so as long as water and oxygen are excluded. Solid state SQUID magnetization measurements (at 1 T) of **1** confirmed a high-spin S = 1 vanadium(III) center with an invariable average μ_{eff} = 2.81 μ_B over a temperature range of 4−300 K (Figure S1). Simulation based on a best fit of the data points in the range 2−200 K yielded the following parameters: S = 1, g_{iso} = 1.95, D = 4.00 cm^{-1}, with a temperature independent paramagnetism (TIP) = 141 × 10^{-6} emu.[42]

Scheme 1. Syntheses of All Described Vanadium Complexes from the (nacnac)VCl(ODiiP) Precursor, 1

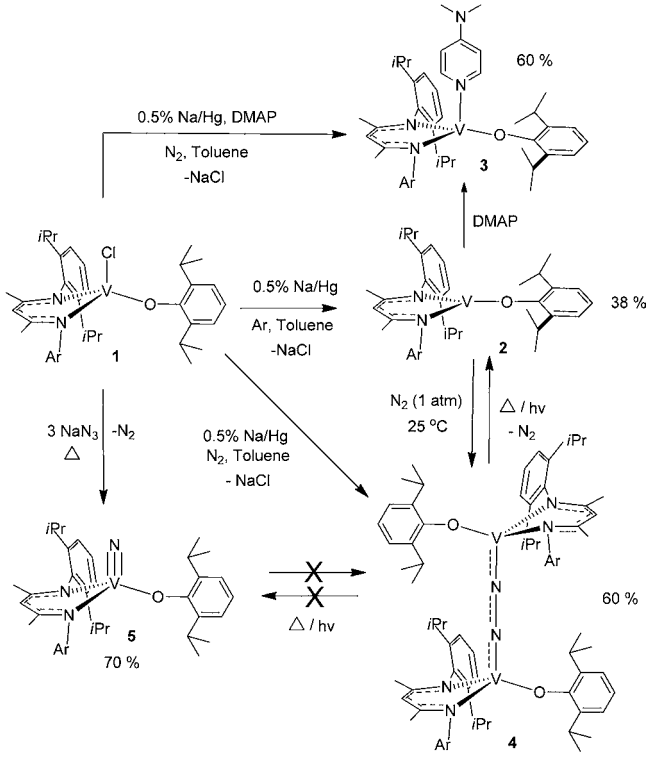

Cyclic voltammetry studies of **1** (0.3 M solution of TBAPF$_6$ in THF) showed a reversible vanadium(III/II) cathodic wave at −2.14 V versus the FeCp$_2$/FeCp$_2^+$ reference at 0.0 V (Figure S2).[42] Chemical reduction of **1** with 0.5% Na/Hg under argon afforded a novel three-coordinate vanadium complex [(nacnac)V(ODiiP)] (**2**) (Scheme 1) as a brown solid in 38% isolated yield via crystallization from a saturated *n*-pentane solution cooled to −37 °C. The XRD of **2**, shown in Figure 1, reveals a rare example of a trigonal planar geometry with overall C_{2v} symmetry in which the mirror plane bisects the nacnac γ-carbon, vanadium center, and aryloxide ligand. Metrical parameters about the (nacnac)V(II) scaffold in **2** are V1−N1, 2.000(2) Å; V1−O1, 1.836(2) Å; N1′−V−N1′, 86.72(6)°, which are similar to that observed in zwitterion complex [(nacnac)V(η^6-PhBPh$_3$)].[43] Moreover, the aryloxide ligand coordinates to the vanadium in a linear fashion suggestive of π donation into the unsaturated vanadium center. This type of coordination behavior between T- versus Y-shaped geometries has been predicted by DFT with (nacnac)M(II) systems (M = Cr,[44] Fe,[45,46] Co,[45] Ni,[45,47] Cu[48,49]) with monoanionic σ and π donors.

Solid-state SQUID magnetization measurements of **2** over the temperature range of 2−300 K are consistent with an S = $^3/_2$ species (Figure 2). The average magnetic moment of μ_{eff} = 3.77 μ_B is similar to that of [(nacnac)V(Ntolyl$_2$)] and is

dx.doi.org/10.1021/ja303360v | J. Am. Chem. Soc. 2012, 134, 13035−13045

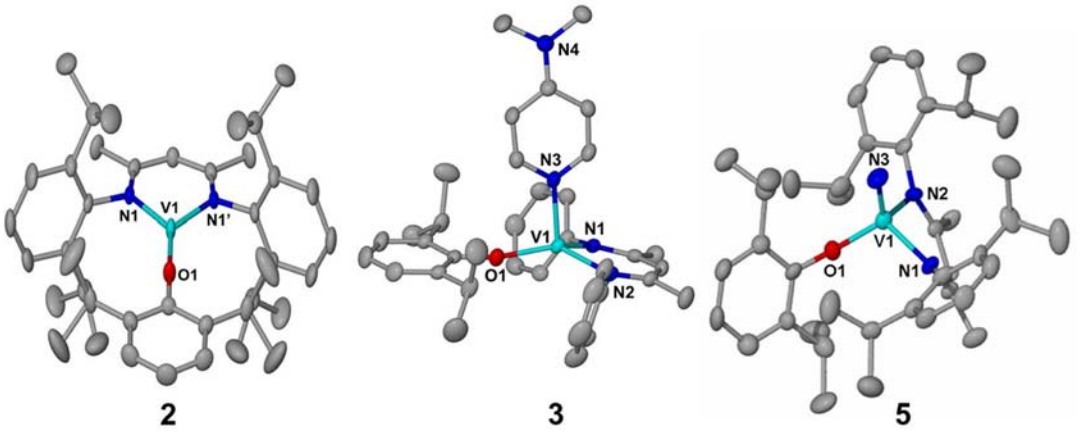

Figure 1. Molecular structures of [(nacnac)V(ODiiP)] (**2**), [(nacnac)V(DMAP)(ODiiP)] (**3**), and [(nacnac)V≡N(ODiiP)] (**5**) are shown with thermal ellipsoids depicted as 50% probability. All hydrogen atoms have been omitted for clarity. Selected bonds (Å) and angles (°) for **2**: V(1)−N(1) = 2.000(2), V(1)−O(1) = 1.836(2); N(1)−V(1)−N(1′) = 86.72(6), N(1)−V(1)−O(1) = 136.56(6), V(1)−O(1)−C(ipso) = 177.46(5). For **3**: V(1)−N(1) = 2.054(3), V(1)−N(2) = 2.058(3), V(1)−N(3) = 2.096(2), V(1)−O(1) = 1.925(2); N(1)−V(1)−N(2) = 87.79(10), N(1)−V(1)−O(1) = 125.62(9), N(2)−(1)−O(1) = 131.97(10), N(1)−V(1)−N(3) = 107.41(10), N(3)−V(1)−O(1) = 95.33(9), V(1)−O(1)−C(ipso) = 166.66(19). For **5**: V(1)−N(1) = 1.956(3), V(1)−N(2) = 1.947(4), V(1)−N(3) = 1.565(4), V(1)−O(1) = 1.814(3), N(1)−V(1)−N(2) = 97.85(15), N(1)−V(1)−N(3) = 110.58(17), N(1)−V(1)−O(1) = 109.46(14), N(3)−V(1)−O(1) = 114.76(18), V(1)−O(1)−C(ipso) = 150.4(3).

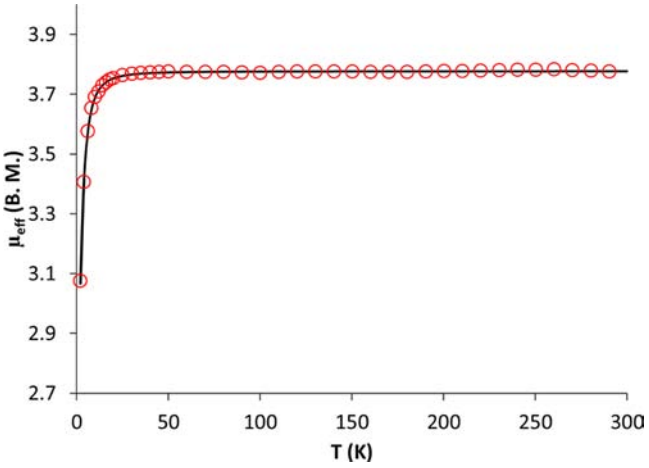

Figure 2. Temperature-dependent DC susceptibility of a powder of **2** measured at 1 T (red circles) with a simulation (black line) in the range 2−300 K using the following best-fitted parameters: $S = {}^3/_2$, $g_{iso} = 1.94$, $D = 3.75$ cm^{-1}.

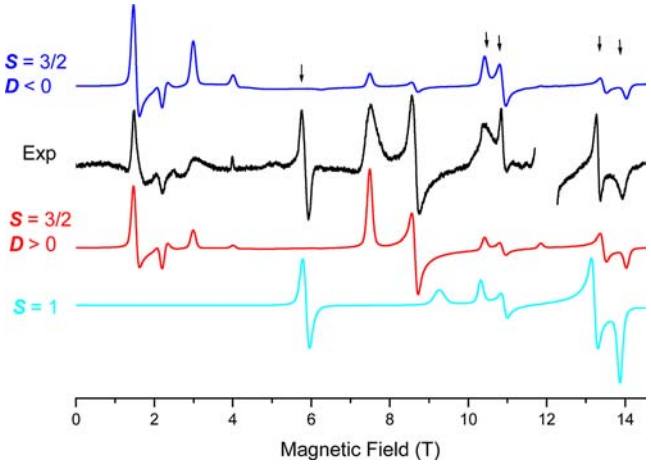

Figure 3. HFEPR spectrum of a polycrystalline sample of **2** recorded at 10 K and 328.8 GHz (black trace) with the V(IV) impurity resonance at 12 T left out. Arrows point at resonances attributed to a superposition of V(II) turning points and those originating from a V(III) ($S = 1$) impurity. Simulations for **2** are provided employing the spin Hamiltonian parameters as in text (blue trace, $D < 0$; red trace, $D > 0$). The cyan trace is a simulation of the V(III) impurity using: $S = 1$, $g_{iso} = 1.93$, $D = -2.62$ cm^{-1}, $E = -0.186$ cm^{-1}.

invariant over 25−300 K. This value is also comparable to the magnetic moment of 3.83 μ_B at 25 °C obtained in solution by the Evans method. In the solid state, the magnetic moment sharply decreases below 20 K due to zero-field splitting (zfs). The magnetization data were fitted using a standard spin Hamiltonian for $S = {}^3/_2$ and an axial zfs parameter of $D = 3.75$ cm^{-1} and $g_{iso} = 1.94$ (Figure 2). Multifrequency HFEPR measurements of powdered samples at low temperatures were also consistent with a mononuclear complex having a quartet ground state (Figure 3). Although the spectra show trace amounts of V(III) and V(IV) impurities, the dominant signals are clearly indicative of an $S = {}^3/_2$ ground state. Even if the agreement between single-frequency spectra and their simulations could be already deemed very good, the actual spin Hamiltonian parameters were obtained by least-squares fitting of the resonance field versus microwave frequency dependencies measured over a wide frequency range, as shown in the two-dimensional map of EPR resonances in Figure 4.[50] The following spin Hamiltonian parameters were obtained from the fits: $S = {}^3/_2$; $|D| = 4.066(10)$ cm^{-1}, $|E| = 0.225(5)$ cm^{-1}; $g = [1.960(4), 1.932(3), 1.979(9)]$. The sign of D was proved positive by simulating single-frequency spectra, as shown in Figure 3. The spin Hamiltonian parameters stand in good agreement with the SQUID data. Complex **2** has a larger D value than any other reported V(II) complex, including prototypical vanadocene systems[51] and the masked three-coordinate complex [(nacnac)V(Ntolyl$_2$)],[10] which we tentatively attribute to its unusual trigonal planar environment.

Given the unsaturated nature of complex **2**, it can readily coordinate one equiv of DMAP (4-dimethylaminopyridine) to form [(nacnac)V(DMAP)(ODiiP)] (**3**) quantitatively. Complex **3** can be prepared more conveniently in 60% yield via Na/Hg reduction of **1** in the presence of DMAP (Scheme 1). Unlike [Mo(N[^{t}Bu]Ar)$_3$], which readily cleaves N_2 in minutes

dx.doi.org/10.1021/ja303360v | J. Am. Chem. Soc. 2012, 134, 13035−13045

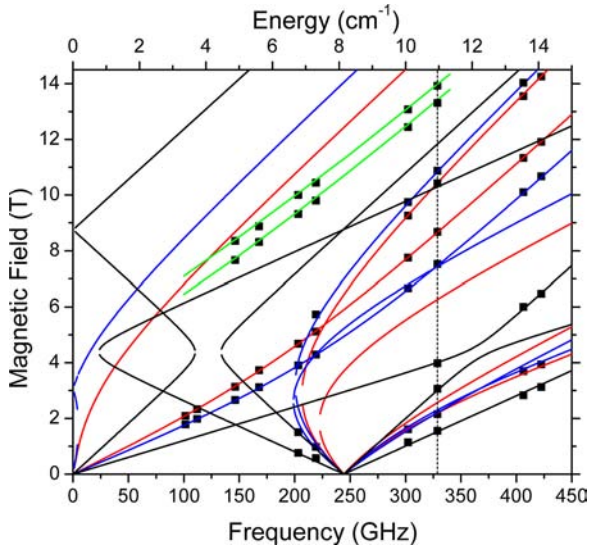

Figure 4. Two-dimensional map of EPR resonances observed in **2** at 10 K. Squares: experimental turning points; curves: simulations using spin Hamiltonian parameters as in the text. Red lines: turning points with $B_0 \| x$; blue: $B_0 \| y$; black: $B_0 \| z$; green: off-axis turning points. The dashed line represents the frequency at which the spectrum shown in Figure 3 was acquired (328.8 GHz).

at room temperature when exposed to DMAP or other *N*-heterocyclic donors, the adduct **3** is far less reactive than precursor **2**.[4] The Evans susceptibility measurement of **3** is 3.79 μ_B, in good agreement with a high-spin vanadium(II) complex, analogous to **2**. An XRD structural analysis of **3** shows a very similar N_2VO scaffold (N_2 = nacnac, *O* = ODiiP) when compared to **2** (Figure 1). On the contrary, when exposed to an atmosphere of N_2, a benzene solution of complex **2** gradually and quantitatively engendered a new compound over 6 h based on ^{1}H NMR spectroscopy (Scheme 1). Recrystallization of the crude product from a saturated solution of *n*-pentane at −37 °C yielded a dark brown microcrystalline compound. XRD studies identified this new species to be the end-on dinitrogen divanadium complex [(nacnac)(ODiiP)V]$_2$(μ_2-η^1:η^1-N_2) (**4**) (Figure 5). Unfortunately, a satisfactory refinement model could not be found for the diffraction data so we refrain from commenting on any metrical parameters. Nevertheless all salient features indicate some degree of N_2 reduction and formation of a topologically linear V=N=N=V core.

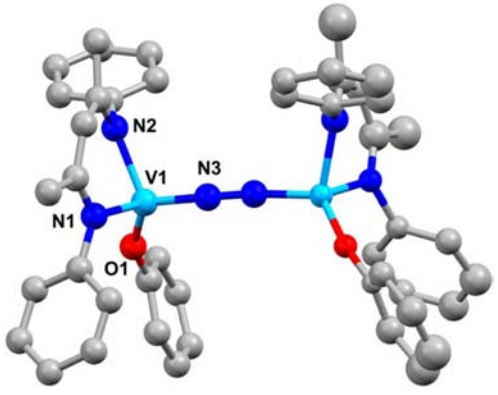

Figure 5. Ball and stick representation of the disordered solid state structure of **4** with ^{i}Pr groups and H-atoms omitted for clarity.

Raman vibrational spectra of **4** also corroborate substantial N≡N bond reduction, since a sharp peak is observed at 1374 cm^{-1} which shifts to 1330 cm^{-1} when the $^{15}N_2$ isotopologue [(nacnac)(ODiiP)V]$_2$(μ_2-η^1:η^1-$^{15}N_2$) is prepared from 98% enriched $^{15}N_2$.[39,52] Taken together, the Raman data and the solid-state structure suggest a significant reduction of the N−N bond order when compared to free dinitrogen, which is characterized by ν_e/c = 2358 cm^{-1}. Exposure of the $^{15}N_2$ isotopologue of **4** to a dinitrogen atmosphere over 24 h at 25 °C shows no exchange with unlabeled N_2. In fact, compound **4** is indefinitely stable at room temperature as a solid or in solution, which contrasts the lability of N_2 in unstable V(III) dinitrogen systems that expel this ligand especially upon dissolution.[34,37] Alternatively, the reduction of **1** with 0.5% Na/Hg in toluene for 6 h under a dinitrogen atmosphere also rendered formation of **4** in 60% isolated yield and without need to isolate the reactive complex **2** (Scheme 1). To our surprise, SQUID magnetization measurements of **4** suggest that this complex is diamagnetic, corroborated by NMR spectroscopic experiments. The ^{1}H NMR (d_8-toluene) spectra collected between 25 and −80 °C, show no changes in the relatively sharp resonances that fall well within the diamagnetic region (0−12 ppm). ^{51}V NMR (C_6D_6, 25 °C) spectroscopy reveals an intense resonance at 167.4 ppm ($\Delta\nu_{1/2}$ = 500 Hz, Figure S8).[42] Multiple attempts to observe an ^{15}N NMR resonance for the $^{15}N_2$ enriched isotopomer of **4** were unsuccessful presumably due to broadening because of coupling to ^{51}V (I = 7/2, 99.75%) and ^{14}N nuclei (I = 1, 99.636%). Therefore, our data alludes that complex **4** has two vanadium(III) centers that are antiferromagnetically (AF) coupled to yield an overall diamagnetic (S = 0) system with S = 1, 2 excited spin states. Solid state SQUID measurements of crystalline **4** were inconclusive presumably due to its diamagnetic nature. As a result, we relied on variable temperature HFEPR spectroscopy (between 150 and 300 K) collected at a frequency of 211 GHz. At temperatures above 200 K, a thermally activated triplet system is observed (albeit in low concentrations, ∼1%), which is most probably an excited spin state of the dinuclear complex **4** (Figure S9).[42] Simulation of the spectra yielded small zfs parameters: D = 0.75 cm^{-1}, E = 0.056 cm^{-1}, and the intensity of the signal decayed as the temperature was lowered suggesting complex **4** to have a singlet ground state. The quintet was never observed under the above conditions. The cyclic voltammogram of complex **4** displays a reversible cathodic wave at −1.37 V (top of Figure 6) with a peak-to-peak separation of 82 mV implying minimal rearrangement within the structural framework upon introduction of a single electron to form the radical anion **4**$^-$. The linear dependence of the current versus the square root of the scan rate confirms the reversibility of the electron transfer (bottom of Figure 6). A second, but irreversible cathodic wave is observed at −2.62 V (Figure S5).[42] Complex **4** also displays an irreversible anodic wave at 0.55 V and scanning faster did not deflect the irreversibility.

Surprisingly, complex **4** does not cleave the triple bond of dinitrogen to afford the nitride complex [(nacnac)V≡N(ODiiP)] (**5**), despite the system having six electrons available from the two V(II) ions to populate all the π^* and σ^* MO's of N_2. Monitoring the thermolysis of **4** at 90 °C in d_6-benzene by ^{1}H NMR spectroscopy led to regeneration of **2** within 1 h. Moreover, photolysis experiments also liberated N_2 albeit more sluggishly (3 h for complete displacement of N_2)

dx.doi.org/10.1021/ja303360v | J. Am. Chem. Soc. 2012, 134, 13035−13045

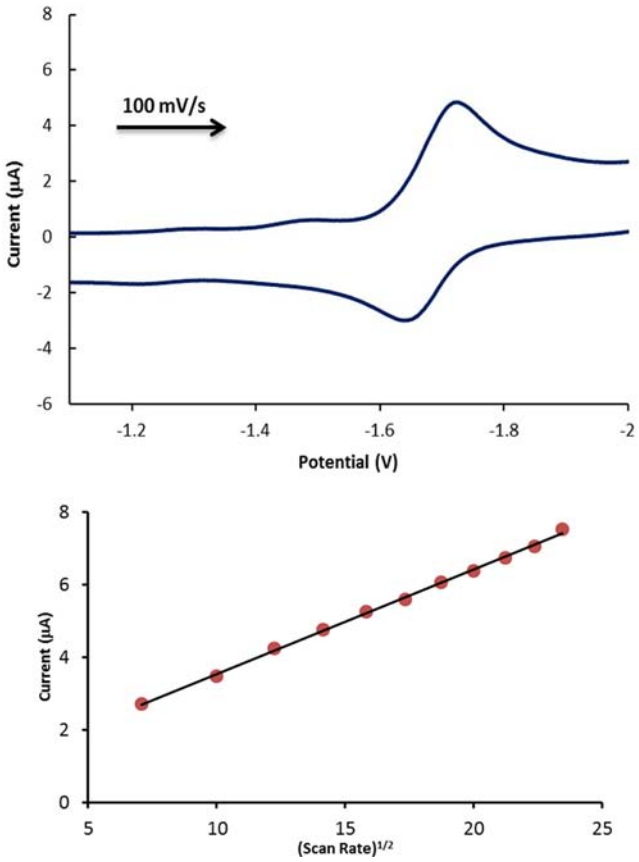

Figure 6. (Top) Cyclic voltammogram of complex **4** in a 0.30 M of solution of $[NBu_4][PF_6]$ in anhydrous THF solution at a scan rate of 100 mV/s. (Bottom) Linear dependence of current versus scan rate$^{1/2}$.

and yielded no detectable vanadium nitride as evinced by ^{1}H NMR spectroscopy or high resolution mass spectrometry. Using excess amounts of reducing agents also failed to generate a nitride product from **4**. To understand why complex **4** did not fragment into the corresponding nitride complex **5**, we prepared the latter compound independently from **1** and NaN_3 in 70% yield (Scheme 1). Complex **5** has been fully characterized by multinuclear (^{1}H, ^{13}C, ^{15}N, and ^{51}V) NMR, FT-IR, and combustion analysis.[42] Notably, complex **5** is a rare example of a mononuclear, and neutral four-coordinate vanadium nitride.[10,53] The V≡N functionality for **5** has been unequivocally identified by infrared spectroscopy with an intense stretch at 1024 cm^{-1}, which in the isotopically enriched **5**-^{15}N (from 50% enriched NaN_3) shifts to 998 cm^{-1}. A ^{15}N NMR (C_6D_6, 25 °C) spectrum of **5**-^{15}N confirmed a highly deshielded terminal nitride moiety at 1059 ppm ($\Delta\nu_{1/2}$ = 36 Hz, Figure S7).[54] At 25 °C, the ^{1}H NMR (d_8-toluene) spectrum of **5** revealed broad resonances resulting from rapid rotation of the aryloxide ligand, but cooling of the solution to −40 °C resolved all assignable resonances.[42] The molecular structure of **5**, shown in Figure 1, clearly displays the presence of a terminal nitride ligand at 1.565(4) Å, in which the bond distance is comparable to the few known mononuclear vanadium nitride complexes.[55−59] The geometry of **5** is that of a distorted tetrahedron as judged by the N3−V1−O1 angle of 114.76(18)°. The V1−O1−C(ipso) angle is bent at 150.4(3)° suggestive of pseudo-σ ligation. Overall, metrical parameters in the molecular structure of **5** resemble the nitride derivative [(nacnac)V≡N(N[R]tol)] (*R* = tol or 2,4,6-$Me_3C_6H_2$) that we reported recently.[10,53] Although we can prepare the nitride, attempts to convert **5** to **4** by chemical reduction, photolysis, or thermolysis have been unsuccessful.

We turned to DFT calculations to address questions concerning the inability of our vanadium system to cleave dinitrogen, and to gain insight into the electronic structure of **4** to explain its unusual magnetism. Figure 7 illustrates the computed solution phase free energy reaction coordinate involving complex **2** and N_2, and its conversion to **5** via intermediates [(nacnac)V(ODiiP)(N_2)] (**2**-N_2), and **4**, as well as the zigzag-like transition state structure **4-TS**. All computed structures use a truncated version where the ^{i}Pr on the nacnac ligand have been replaced with a methyl group. Metrical parameters for the most salient features of these compounds are listed in the caption of Figure 7 and the computed structures for complexes **2** and **5** are in good agreement with the metrical parameters obtained from the crystallographic data. Our calculations suggest that complex **2** and N_2 first form a terminal end-on N_2 adduct, **2**-N_2, with a minimal energy difference of 2.0 kcal mol^{-1} to the reactants. Coordination of the second equivalent of **2** to **2**-N_2 produces the divanadium-N_2 bridged product **4** with a relative energy of −16.0 kcal mol^{-1}.[60] As noted from spectroscopic and magnetic studies, complex **2** has a quartet ground state that we calculate to be 24.8 kcal mol^{-1} lower in energy than the doublet state. However, spin-flip occurs during the association of **2** and N_2 to form the doublet species **2**-N_2.[61] Up to this point, the reactivity of **2** mirrors that of complex [Mo(N[^{t}Bu]Ar)$_3$].[2,3,5] However, Figure 7 shows disappointingly that conversion of complex **4** to **5** is associated with a prohibitively high barrier: 83 kcal mol^{-1}. Similarly, the reductive coupling of two equivalents of **5** into one **4**, that is, the reverse reaction, is also associated with an extremely high activation energy of 50.79 kcal mol^{-1}. These results are in agreement with the experimental observations that **4** does not convert into **5** and *vice versa*.[62] As shown in Figure 7,

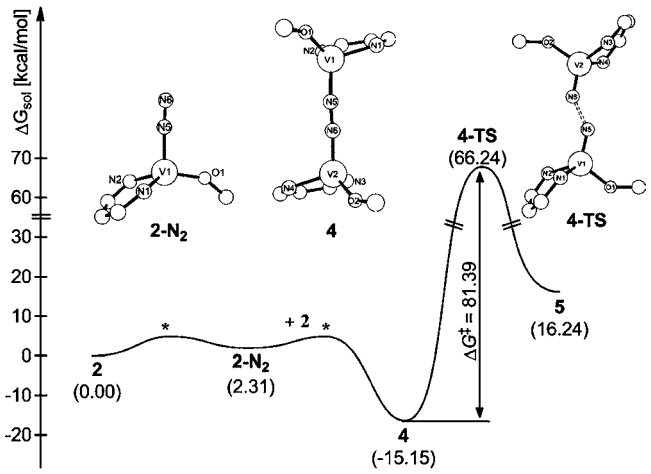

Figure 7. Computed reaction profile from **2** to **4** and then to the nitride **5**. Computed structures of **2**-N_2, **4** and **4-TS** are shown with aryl groups and the nacnac β-methyl omitted for the purpose of clarity. Distances are reported in Å and angles in degrees. Some computed metrical parameters for **2**-N_2: V1−N1, 1.972; V1−N2, 1.973; V1−N5, 1.950; V1−O1, 1.842; N5−N6, 1.130; V1−N5−N6, 176.85. For **4**: V1−N1, 2.011; V1−N2, 2.024; V1−N5, 1.836; V1−O1, 1.836; N5−N6, 1.204; V1−N5−N6, 175.06; V2−N6−N5, 175.24. For **4-TS**: V1−N1, 1.989; V1−N2, 1.988; V1−N5, 1.613; V1−O1, 1.818; N5−N6, 1.675; V1−N5−N6, 143.26; V2−N6−N5, 143.30.

dx.doi.org/10.1021/ja303360v | J. Am. Chem. Soc. 2012, 134, 13035−13045

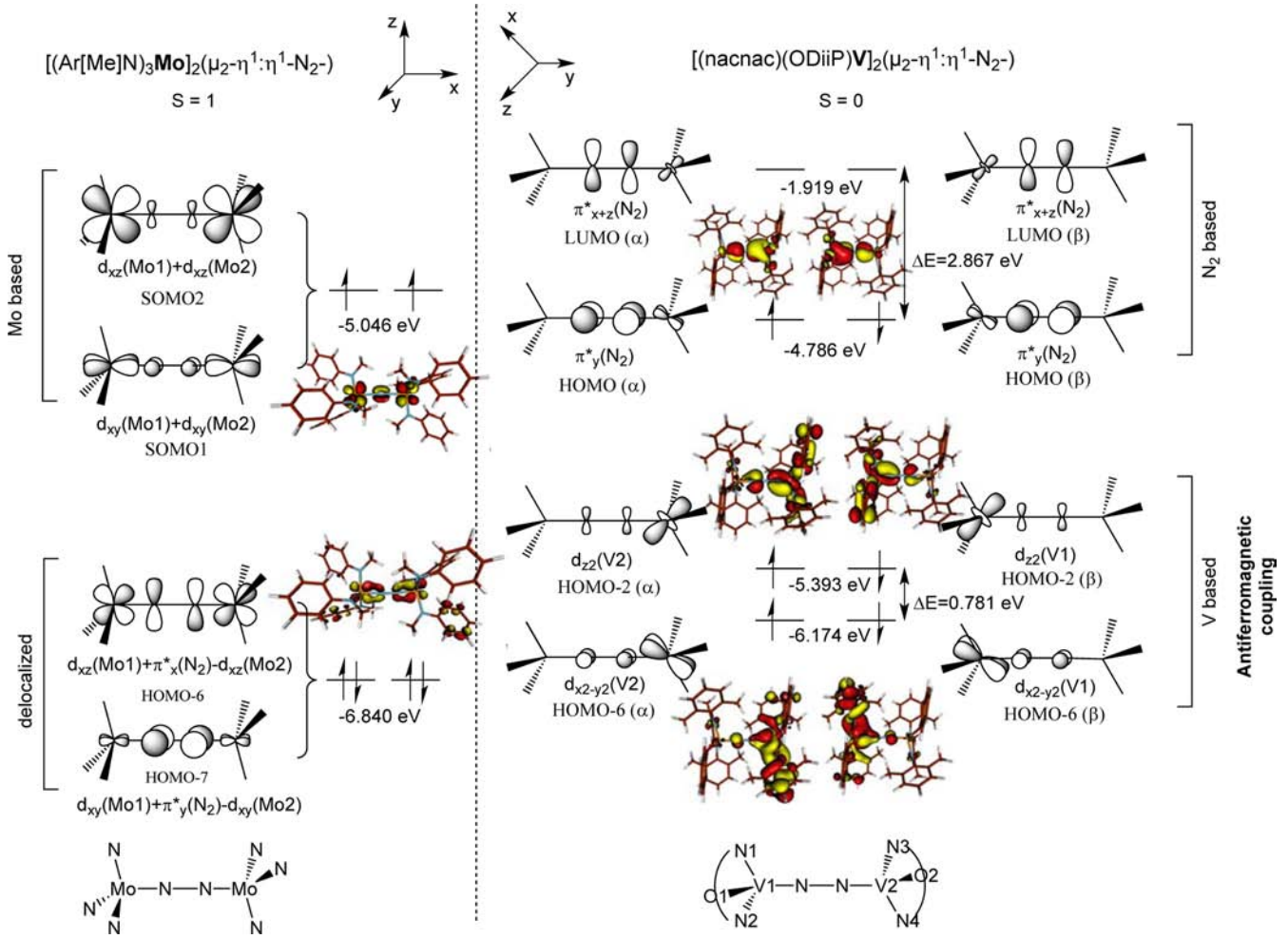

Figure 8. Molecular orbitals representing the main differences between the electronic structure of triplet **Mo** and AF coupled **4**. Only the most important π type orbitals are shown. Due to the small pyramidalization around the Mo centers, d orbitals are D_{3h}/ML_3 like in **Mo** whereas they resemble the d orbitals are in a tetrahedral field in **4**. Note the different axis systems, accordingly, to follow conventions.

the reactive nitride **5** lies higher in solution phase energy than **4** and the starting material **2**: a striking contrast to the dominant thermodynamic stability of $[N{\equiv}Mo(N[^tBu]Ar)_3]$ over $[Mo(N[^tBu]Ar)_3]$.[1−5] In accord with the structure of **4**, the optimized geometry also adopts a *gauche* conformation with a dihedral angle of ∠O1−V1−V2−O2 = 69.5° and with only slight bending of the V−N−N−V (∠V1−N5−N6 = 175.2°) moiety (Figure 7).[42] Our calculations also predict complex **4** to possess two AF coupled metal centers that result in an overall singlet ground state lying about 6 and 50 kcal mol^{-1} lower in solution-phase free energy than the lowest triplet and closed shell singlet states, respectively (Figure S11). As noted previously, our HFEPR data at high temperature are in agreement with complex **4** populating the triplet state. Despite the metals being isovalent, the resting state electronic structure of **4** differs profoundly from that of complex $[(Ar[^tBu]N)_3Mo]_2(\mu_2\text{-}\eta^1{:}\eta^1\text{-}N_2)$ (**Mo**) (Figure 8).[2,5] The latter has a triplet ground state, in which four of the six π electrons are paired and occupy the strongly delocalized $\pi^*(N_2)$-$e_g(Mo)$ bonding combinations (HOMO-6 and HOMO-7), whereas the remaining two electrons stay unpaired and are delocalized between the two Mo centers[2] (SOMO1 and SOMO2).[23] In **4**, however, the d_{z^2} and $d_{x^2-y^2}$ orbitals lie significantly lower in energy than the π^* of N_2 resulting in weak orbital interaction and metal based bonding configurations. Mulliken spin density calculations of **4** show significant excess α-spin density of 2.1 and 0.4 on V1 and N6 matched by the same excess of β-spin density on V2 and N5, respectively. These values indicate that **4** contains two AF coupled vanadium(III) centers and a doubly reduced N_2^{2-} ligand bridging the vanadium centers. The Wiberg bond index of 1.82 for N_2 is consistent with $^-N{=}N^-$ type ligand, further supporting our assignment. Within the Broken Symmetry Orbital approach, the different α and β orbitals located on V2 and V1 illustrate the AF coupling of the two V(III) centers (HOMO-2 and HOMO-6) through the N_2^{2-} bridge via a superexchange mechanism. In addition, due to the *gauche* arrangement of the OAr groups and the difference in the ligand strength of the nacnac and ODiiP ligands, the N_2 based π^* MOs are not degenerate in **4** (Figure 8), which facilitates the pairing of the remaining two π electrons in the lower lying $\pi^*(N_2)$ (HOMO). The departure in the electronic structures of **4** and **Mo** stems from the different interaction between the π^* orbitals of the N_2 moiety and the d orbitals of the metal centers: in **4**, the d_{z^2} and $d_{x^2-y^2}$ are involved, whereas d_{xy} and d_{xz} are dominant in the case of the **Mo** complex (Figure 8). Recently, the coexistence of the closed shell singlet and AF coupled singlet states were argued for the four π−electron $\{(RO)_3V\}_2(\mu_2{-}\eta^1{:}\eta^1\text{-}N_2)$ ($R = {}^tBu_2MeC$).[37]

The N_2 fragment in **4** and **Mo** seem similar when judged by their respective bond lengths of 1.20 and 1.19 Å and Wiberg

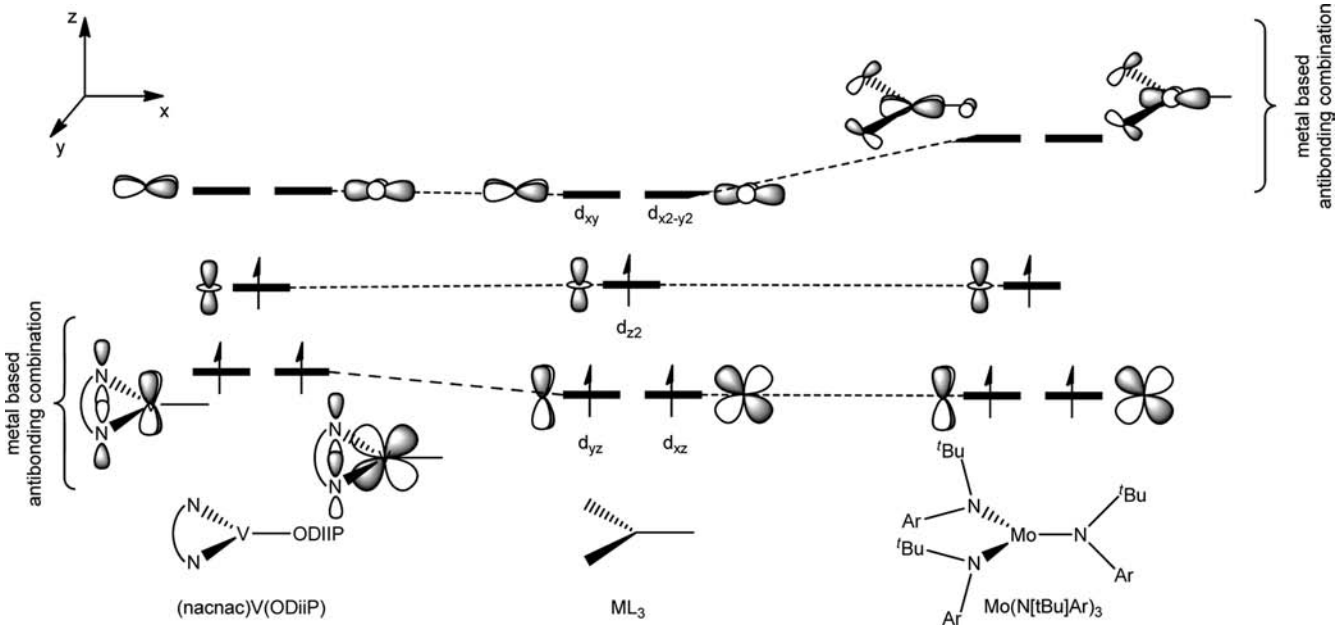

Figure 9. Simplified frontier molecular orbitals of complex **2** and [Mo(N[^{t}Bu]Ar)$_3$]. The low symmetry in **2** renders all orbitals nondegenerate, but for the purpose of simplification, we depict these at similar energy levels. The energy levels for the d-orbitals with purely σ-donors are shown in the middle. Note that orbital energies for Mo and V are different due to effective charges of their cores.

bond indices of 1.82 and 1.85. However, breaking the N−N bond is much more difficult in **4** than in **Mo** with the respective computed barriers, $\Delta G^{\ddagger}$ = 83.0 kcal mol^{-1}and $\Delta G^{\ddagger}$ = 20.8 kcal mol^{-1}. The prerequisite for the N−N bond breaking is that the N_2 based antibonding orbitals are appreciably filled: two $\pi^*(N_2)$ orbitals as well as the $\sigma^*(N_2)$ orbital. To utilize the available six π electrons for such purposes, these systems have to undergo geometrical alterations that allow the transition between π and σ subspaces. The transition state **4-TS** must adopt a zigzag geometry, as shown in Figure 7, which is a salient feature already characterized for the analogous molybdenum systems.[2,63−68] The contrast in reactivity is rather surprising since analysis of the frontier orbitals of **2** and [Mo(N[^{t}Bu]Ar)$_3$] reveal subtle differences in the bonding scheme. Figure 9 depicts a comparison of their frontier orbitals, paying close attention to the π-component resulting from the contrast of the nacnac ligand from the anilide. As shown in Figure 9, the π^* set in [Mo(N[^{t}Bu]Ar)$_3$] is more destabilized than in **2**, due to the presence of two linear combinations resulting from the anilide *in-plane* π-donor set. In contrast, complex **2** does not provide such a combination, and the nacnac π-framework results in a slight destabilization of the d_{xz} and d_{yz} orbitals, with the d_{xy} and $d_{x^2-y^2}$ orbitals remaining essentially intact. Not surprisingly, the d_{z^2} orbital remains the same for both systems consistent with the planar, three-coordinate environment being retained in both V(III) and Mo(III). Although complexes **2** and [Mo(N-[^{t}Bu]Ar)$_3$] are not isolobal, they are not too dissimilar considering the presence of the nacnac ligand framework. The only main difference is that complex **2** is more electron deficient as a result of lacking in-plane π-donor ligands (in the xy axis).

CONCLUSIONS

Our work reports the first example of a discrete three-coordinate V(II) complex **2**, as well as some of its preliminary reactivity. We show that this complex can serve as a template for small molecule activation, including the formation of a bridging end-on dinitrogen complex **4**, and gives access to the terminal nitride complex **5**, but unfortunately not from N_2. Our work also demonstrates that access to the nitride from dinitrogen is both thermally and kinetically prohibited. This difficulty is imparted both by the weaker d−π^* interaction of vanadium with nitrogen in **4** (as N_2) and **5** (as N^{3-}) as well as the larger structural change needed to achieve the zigzag-like transition state en route to formation of the nitride. The more constrained geometry in **2**, imparted by the less flexible, chelating nacnac ligand, might be precluding such a distortion to achieve a zigzag-like structure. We speculate that distortion of the molecule (such as ligand rotation) is a necessity for electron pairing in the intersystem crossing. As a result, more rigid conformations prevent cooperative N_2 splitting such as in the case of [N_3N]Mo (N_3N^{3-} = [RNCH$_2$CH$_2$]$_3$N, R = Me$_3$Si, *t*-BuMe$_2$Si, C_6F_5).[69−71] We are presently investigating how to manipulate and understand the latter process since it appears to be a key step in dinitrogen cleavage. Being able to generate vanadium nitrides from N_2 will provide an opportunity to exploit the nitride group since these species are not as thermodynamically stable as the molybdenum counterparts.

ASSOCIATED CONTENT

Supporting Information

X-ray crystallographic information, computational information, magnetic data and spectral data are provided. This material is available free of charge via the Internet at http://pubs.acs.org.

AUTHOR INFORMATION

Corresponding Author

*mindiola@indiana.edu

Notes

The authors declare no competing financial interest.

ACKNOWLEDGMENTS

We thank the Chemical Sciences, Geosciences and Biosciences Division, Office of Basic Energy Science, Office of Science, U.S.

Department of Energy (no. DE-FG02-07ER15893), as well as the NHMFL, which is funded by the NSF through Cooperative Agreement no. DMR-0654118, the State of Florida, and the DOE for financial support. D.J.M. acknowledges support from the Alexander von Humbold Stiftung. A.J.N. acknowledges Indiana University STARS program for a summer fellowship. K.M. thanks the Deutsche Forschungsgemeinschaft (DFG SFB 583) and the University of Erlangen for financial support. We thank Dr. Edward H. Witlicki and the Flood group for assistance with the Raman measurements.

■ REFERENCES

(1) Laplaza, C. E.; Cummins, C. C. *Science* **1995**, *268*, 861.
(2) Laplaza, C. E.; Johnson, M. J. A.; Peters, J. C.; Odom, A. L.; Kim, E.; Cummins, C. C.; George, G. N.; Pickering, I. J. *J. Am. Chem. Soc.* **1996**, *118*, 8623.
(3) Peters, J. C.; Cherry, J.-P. F.; Thomas, J. C.; Baraldo, L.; Mindiola, D. J.; Davis, W. M.; Cummins, C. J. *J. Am. Chem. Soc.* **1999**, *121*, 10053.
(4) Tsai, Y.-C.; Cummins, C. C. *Inorg. Chim. Acta* **2003**, *345*, 63.
(5) Curley, J. J.; Cook, T. R.; Reece, S. Y.; Muller, P.; Cummins, C. C. *J. Am. Chem. Soc.* **2008**, *130*, 9394.
(6) Ferguson, R.; Solari, E.; Floriani, C.; Osella, D.; Ravera, M.; Re, N.; Chiesi-Villa, A.; Rizzoli, C. *J. Am. Chem. Soc.* **1997**, *119*, 10104.
(7) Shilov, A.; Denisov, N.; Efimov, O.; Shuvalov, N.; Shuvalova, N.; Shilova, A. *Nature* **1971**, *231*, 460.
(8) Zones, S. I.; Vickery, T. M.; Palmer, J. G.; Schrauzer, G. N. *J. Am. Chem. Soc.* **1976**, *98*, 1289.
(9) Zones, S. I.; Palmer, M. R.; Palmer, J. G.; Doemeny, J. M.; Schrauzer, G. N. *J. Am. Chem. Soc.* **1978**, *100*, 2113.
(10) Tran, B. L.; Singhal, M.; Park, H.; Lam, O. P.; Pink, M.; Krzystek, J.; Ozarowski, A.; Telser, J.; Meyer, K.; Mindiola, D. J. *Angew. Chem., Int. Ed.* **2010**, *49*, 9871.
(11) Chiu, H.-T.; Chen, Y.-P.; Chuang, S.-H.; Jen, J.-S.; Lee, G.-H.; Peng, S.-M. *Chem. Commun.* **1996**, 139.
(12) Tran, B. L.; Chen, C.-H.; Mindiola, D. J. *Inorg. Chim. Acta* **2011**, *369*, 215.
(13) Budzelaar, P. H. M.; Oort, A. B. v.; Orpen, A. G. *Eur. J. Inorg. Chem.* **1998**, 1485−1494.
(14) Evans, D. F. *J. Chem. Soc.* **1959**, 2003.
(15) Bain, G. A.; Berry, J. F. *J. Chem. Educ.* **2008**, *85*, 532.
(16) Hassan, A. K.; Pardi, L. A.; Krzystek, J.; Sienkiewicz, A.; Goy, P.; Rohrer, M.; Brunel, L.-C. *J. Magn. Reson.* **2000**, *142*, 300.
(17) In *Jaguar 7.0*; Schrödinger LLC: New York, 2007.
(18) Becke, A. D. *J. Chem. Phys.* **1993**, *98*, 5648.
(19) Becke, A. D. *Phys. Rev. A* **1988**, *38*, 309858.
(20) Vosko, S. H.; Wilk, L.; Nusair, M. *Can. J. Phys.* **1980**, *58*, 1200.
(21) Lee, C. T.; Yang, W. T.; Parr, R. G. *Phys. Rev. B* **1988**, *37*, 785.
(22) Wadt, W. R.; Hay, P. J. *J. Chem. Phys.* **1985**, *82*, 284.
(23) Hay, P. J.; Wadt, W. R. *J. Chem. Phys.* **1985**, *82*, 270.
(24) Dunning, T. H. *J. Chem. Phys.* **1989**, *90*, 1007.
(25) Marten, B.; Kim, K.; Cortis, C.; Friesner, R. A.; Murphy, R. B.; Ringnalda, M. N.; Sitkoff, D.; Honig, B. *J. Chem. Phys.* **1996**, 100.
(26) Friedrichs, M.; Zhou, R. H.; Edinger, S. R.; Friesner, R. A. *J. Chem. Phys. B* **1999**, *103*, 3057.
(27) Edinger, S. R.; Cortis, C.; Shenkin, P. S.; Friesner, R. A. *J. Chem. Phys. B* **1997**, *101*, 1190.
(28) Rashin, A. A.; Honig, B. *J. Chem. Phys. B* **1985**, *89*, 5588.
(29) Noodleman, L. *J. Chem. Phys.* **1981**, *74*, 5737.
(30) Noodleman, L.; Davidson, E. R. *J. Chem. Phys.* **1986**, *109*, 131.
(31) Noodleman, L.; Lovell, T.; Han, W.-G.; Li, J.; Himo, F. *Chem. Rev.* **2004**, *104*, 459.
(32) Halgren, T. A.; Lipscomb, W. N. *Chem. Phys. Lett.* **1977**, *49*, 225.
(33) Peng, C. Y.; Schlegel, H. B. *Isr. J. Chem.* **1993**, *33*, 449.
(34) Edema, J. J. H.; Stauthamer, W.; Bolhuis, F. V.; Gamarotta, S.; Smeets, W. J. J.; Spek, A. L. *Inorg. Chem.* **1990**, *29*, 1302.
(35) Vidyaratne, I.; Crewdson, P.; Lefebvre, E.; Gambarotta, S. *Inorg. Chem.* **2007**, *46*, 8836.
(36) Buijink, J.-K. F.; Meetsma, A.; Teuben, J. H. *Organometallics* **1993**, *12*, 2004.
(37) Groysman, S.; Villagran, D.; Freedman, D. E.; Nocera, D. G. *Chem. Commun.* **2011**, *47*, 10242.
(38) Song, J.-I.; Berno, P.; Gambarotta, S. *J. Am. Chem. Soc.* **1994**, *116*, 6927.
(39) Kilgore, U. J.; Sengelaub, C. A.; Pink, M.; Fout, A. R.; Mindiola, D. J. *Angew. Chem., Int. Ed.* **2008**, *47*, 3769.
(40) Clentsmith, G. K. B.; Bates, V. M. E.; Hitchcock, P. B.; Cloke, F. G. N. *J. Am. Chem. Soc.* **1999**, *121*, 10444.
(41) Bates, V. M. E.; Clentsmith, G. K. B.; Cloke, F. G. N.; Green, J. C.; Jenkin, H. D. L. *Chem. Commun.* **2000**, 927.
(42) See Supporting Information.
(43) Basuli, F.; Kilgore, U. J.; Hu, X.; Meyer, K.; Pink, M.; Huffman, J. C.; Mindiola, D. J. *Angew. Chem., Int. Ed.* **2004**, *43*, 3156.
(44) Fan, H.; Adhikari, D.; Saleh, A. A.; Clark, R. L.; Zuno-Cruz, F. J.; Cabrera, G. S.; Huffman, J. C.; Pink, M.; Mindiola, D. J.; Baik, M.-H. *J. Am. Chem. Soc.* **2008**, *130*, 17351.
(45) Holland, P. L.; Cundari, T. R.; Perez, L. L.; Eckert, N. A.; Lachicotte, R. J. *J. Am. Chem. Soc.* **2002**, *124*, 14416.
(46) Andres, H.; Bominaar, E. L.; Smith, J. M.; Eckert, N. A.; Holland, P. L.; Münck, E. *J. Am. Chem. Soc.* **2002**, *124*, 3012.
(47) Eckert, N. A.; Bones, E. M.; Lachicotte, R. J.; Holland, P. L. *Inorg. Chem.* **2003**, *42*, 1720.
(48) Holland, P. L.; Tolman, W. B. *J. Am. Chem. Soc.* **1999**, *121*, 7270.
(49) Jazdzewski, B. A.; Holland, P. L.; Pink, M.; Victor G. Young, J.; Spencer, D. J. E.; Tolman, W. B. *Inorg. Chem.* **2001**, *2001*, 6097.
(50) Krzystek, J.; Zvyagin, S. A.; Ozarowski, A.; Trofimenko, S.; Telser, J. *J. Magn. Reson.* **2006**, *178*, 174.
(51) (a) Prins, R.; Biloen, P.; van Voorst, J. D. W. *J. Chem. Phys.* **1967**, *46*, 1216. (b) Jacobsen, C. J. H.; Pedersen, E.; Villadsen, J.; Weihe, H. *Inorg. Chem.* **1993**, *32*, 1216. (c) Laurance, N.; Lambe. *J. Phys. Rev.* **1963**, *132*, 1029. (d) Chan, K. K.; Shields, L. *J. Chem. Soc. A* **1970**, 2700. (e) Girolami, G. S.; Wilkinson, G.; Galas, A. M. R.; Thornton-Pett, M.; Hursthouse, M. B. *J. Chem. Soc., Dalton Trans.* **1985**, 1339. (f) Scott, M. J.; Wilisch, W. C. A.; Armstrong, W. H. *J. Am. Chem. Soc.* **1990**, *112*, 2430.
(52) For a recent discussion of dinuclear N_2 complexes having a similar degree of reduction, see: Chomitz, W. A.; Arnold, J. *Chem. Commun.* **2007**, 4797.
(53) Tran, B. L.; Pink, M.; Gao, X.; Park, H.; Mindiola, D. J. *J. Am. Chem. Soc.* **2010**, *132*, 1458.
(54) The highly downfield chemical shift has been correlated to the large chemical shielding anisotropy affiliated with the metal−ligand mutliple bond and its origin has been attributed to the hybridization of a high lying filled σ-symmetry molecular orbital with a low-lying π^* molecular orbital in a 3-fold symmetric environment under an applied magnetic field. (a) Greco, J. B.; Peters, J. C.; Baker, T. A.; Davis, W. M.; Cummins, C. C.; Wu, G. *J. Am. Chem. Soc.* **2001**, *123*, 5003. (b) Wu, G.; Rovnyak, D.; Johnson, M. J. A.; Zanetti, N. C.; Musaev, D. G.; Morokuma, K.; Schrock, R. R.; Griffin, R. G.; Cummins, C. C. *J. Am. Chem. Soc.* **1996**, *118*, 10654.
(55) Willing, W.; Christophersen, R.; Muller, U.; Dehnicke, K. *Z. Anorg. Allg. Chem.* **1987**, *555*, 16.
(56) Critchlow, S. C.; Lerchen, M. E.; Smith, R. C.; Doherty, N. M. *J. Am. Chem. Soc.* **1988**, *110*, 8071.
(57) Song, J.-I.; Gambarotta, S. *Chem.—Eur. J.* **1996**, *2*, 1258.
(58) Henderson, R. A.; Janas, Z.; Jerzykiewicz, L. B.; Richards, R. L.; Sobota, P. *Inorg. Chim. Acta* **1999**, *285*, 178.
(59) Johnson, C. E.; Kysor, E. A.; Findlater, M.; Jasinski, J. P.; Metell, A. S.; Queen, J. W.; Abernethy, C. D. *Dalton Trans.* **2010**, *39*, 3482.
(60) Scans for the approach of N_2 to **2** and for the association of **2**-$\mathbf{N_2}$ with **2** reflect that both processes are barrierless on the potential energy surfaces (PES), in accord with earlier findings for isovalent Mo(N[^{t}Bu]Ar)$_3$ systems. Locating the transition states for the formations of **2**-$\mathbf{N_2}$ and **4** is, unfortunately, impossible with standard

quantum mechanical methods, because entropy plays a pivotal and nontrivial role in determining these transition-state energies (listed with an * in Figure 4).

(61) No stable isomer was found on the quartet PES.

(62) For coupling of terminal metal nitrides to generate N_2, see: (a) Ware, D. C.; Taube, H. *Inorg. Chem.* **1991**, *30*, 4605. (b) Lam, H. W.; Che, C. M.; Wong, K. Y. *J. Chem. Soc., Dalton Trans.* **1992**, 1411. (c) Demadis, K. D.; El-Samanody, E.-S.; Coia, G. M.; Meyer, T. J. *J. Am. Chem. Soc.* **1999**, *121*, 535. (d) Demadis, K. D.; Meyer, T. J.; White, P. S. *Inorg. Chem.* **1997**, *36*, 5678. (e) Newton, C.; Edwards, K. D.; Ziller, J. W.; Doherty, N. M. *Inorg. Chem.* **1999**, *38*, 4032. (f) Seymore, S. B.; Brown, S. N. *Inorg. Chem.* **2002**, *41*, 462. (g) Betley, T. A.; Peters, J. C. *J. Am. Chem. Soc.* **2004**, *126*, 6252. (h) Man, W.-L.; Chen, G.; Yiu, S.-M.; Shek, L.; Wong, W.-Y.; Wong, W.-T.; Lau, T.-C. *Dalton Trans* **2010**, *39*, 11163. (i) Yiu, S.-M.; Lam, W. W. Y.; Ho, C.-M.; Lau, T.-C. *J. Am. Chem. Soc.* **2007**, *129*, 803. (j) Schöffel, J.; Šušnjar, N.a; Nückel, S.; Sieh, D.; Burger, P. *Eur. J. Inorg. Chem.* **2010**, *2010*, 4911. (k) Chan, P.-H.; Chen, S.-P.; Yeung, K.-W.; Yeung, K.-W.; Cheung, K.-C.; Hong, S.; Sun, S.-G.; Wong, K.-Y. *Electrochem. Commun.* **2005**, *7*, 1244. (l) Man, W.-L.; Tang, T.-M.; Wong, T.-W.; Lau, T.-C.; Peng, S.-M.; Wong, W.-T. *J. Am. Chem. Soc.* **2004**, *126*, 478.

(63) Cui, Q.; Musaev, D. G.; Svensson, M.; Sieber, S.; Morokuma, K. *J. Am. Chem. Soc.* **1995**, *117*, 12366.

(64) Christian, G. J.; Stranger, R.; Yates, B. F. *Inorg. Chem.* **2006**, *45*, 6851.

(65) Cavigliasso, G.; Wilson, L.; McAlpine, S.; Attar, M.; Stranger, R.; Yates, B. F. *Dalton Trans.* **2010**, *39*, 4529.

(66) Christian, G. J.; Terrett, R. N. L.; Stranger, R.; Cavigliasso, G.; Yates, B. F. *Chem.—Eur. J.* **2009**, *15*, 11373.

(67) Brookes, N. J.; Graham, D. C.; Christian, G.; Stranger, R.; Yates, B. F. *J. Comput. Chem.* **2009**, *30*, 2146.

(68) Christian, G.; Stranger, R.; Yates, B. F. *Chem.—Eur. J.* **2009**, *15*, 646.

(69) Shih, K.-Y.; Schrock, R. R.; Kempe, R. *J. Am. Chem. Soc.* **1994**, *116*, 8804.

(70) Kol, M.; Schrock, R. R.; Kempe, R.; Davis, W. M. *J. Am. Chem. Soc.* **1994**, *116*, 4382.

(71) O'Donoghue, M. B.; Davis, W. M.; Schrock, R. R. *Inorg. Chem.* **1998**, *37*, 5149.